Final Report for DoE Grant DE-FG02-06ER54878,

Laboratory Studies of Reconnection in Magnetically Confined Plasmas

Jan Egedal, PI

**MIT Physics Department and Plasma Science and Fusion Center
Cambridge, MA, 02139**

1. Executive summary

The Grant DE-FG02-06ER54878, "Laboratory Studies of Reconnection in Magnetically Confined Plasmas", spanned a period 08/31/2006 to 10/31/2009. It partly supported the summer salary of Prof. Egedal as well as two graduate students and material expenses. The grant enabled the operation of a basic plasma physics experiment (on magnetic reconnection) at the MIT Plasma Science and Fusion Center and the MIT Physics Department. A strong educational component characterized this work throughout, with the participation of a large number of graduate and undergraduate students and interns in the experimental activities.

The study of collisionless magnetic reconnection constituted the primary work carried out under this grant. The investigations utilized a configuration developed to be specifically relevant to numerical simulations of magnetic reconnection, allowing the magnetic field-lines to be contained inside the device. The configuration is compatible with the presence of large current sheets in the reconnection region, and reconnection is observed in fast powerful bursts. These reconnection events facilitate the first experimental investigations of the physics governing the spontaneous onset of fast reconnection [12].

In this Report we review the general motivation of this work, the experimental set-up, and the main physics results. The details of the individual chapters are naturally contained in the relevant publications [1-24], indicated in the reference list and annexed to this Report.

2. The problem of magnetic reconnection (from original proposal)

Magnetic reconnection [25] plays a fundamental role in magnetized plasmas as it permits rapid release of magnetic stress and energy through changes in the magnetic field line topology. It controls the spatial and temporal evolution of explosive events such as solar flares, coronal mass ejections, and magnetic storms in the Earth's magnetotail driving the auroral phenomena [26-29]. Because of its unique importance to understanding violent macroscopic phenomena in nearly all magnetized plasmas, reconnection has been the subject of an increasing number of theoretical investigations. Despite the intense research over the past decades, the origin of the fast time scales of collisionless magnetic reconnection is still poorly understood [30]. In recent years it has been shown that so-called two fluid effects (related to the large difference between the electron mass and the ion mass) play an important role in determining the rate of reconnection. However, a detailed understanding of the electron dynamics is still needed to explain the spontaneous onset of reconnection, characteristic for reconnection on the surface of the sun, in the Earth's magnetotail, and in magnetic fusion devices.
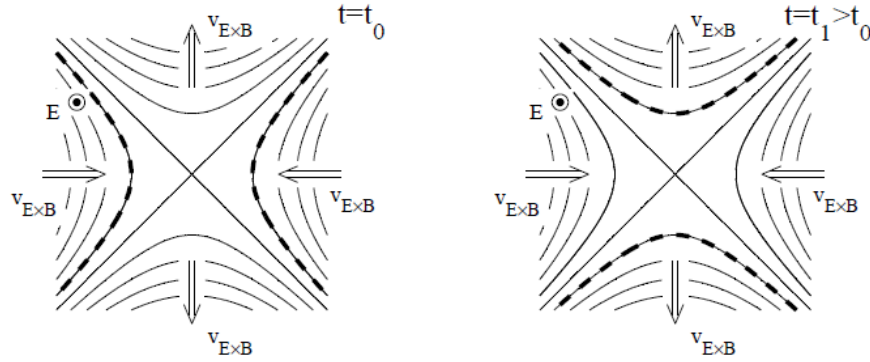

Figure 1: Illustration of the basic geometry for fast magnetic reconnection.

During magnetic reconnection, magnetic field lines in opposing directions cross link and form a magnetic cusp. Such a configuration is characterized by an X-line, a line along which the two components of the magnetic field perpendicular to the line vanish. This basic geometry for fast magnetic reconnection is given in Fig. 1. The sharp gradients and the fine structure in the X-line geometry is thought to cause the breakdown of the theory of resistive-magnetohydrodynamics, which predict, in contradiction to observations, that reconnection is slow in collisionless plasma.

In order to make the reconnection problem numerically and analytically tractable, theoretical investigations often consider a fluid formulation of the plasma dynamics. The most-used theoretical framework for the study of reconnection is the two-fluid plasma description from which the generalized Ohm's law follows

$$\mathbf{E} + \mathbf{v} \times \mathbf{B} = \eta \mathbf{j} + \frac{1}{ne} \left(\mathbf{j} \times \mathbf{B} - \nabla \cdot \mathbf{p}_e \right) + \frac{m_e}{ne^2} \left(\mathbf{v} \cdot \nabla \mathbf{j} + \frac{\partial \mathbf{j}}{\partial t} \right)$$

(1)

Theoretical models for reconnection have been developed in which one or more of the terms on the right hand side of equation (1) are elected to be responsible for breaking the so-called ideal plasma "frozen-in law." As an example, the well-known Sweet-Parker reconnection model [31, 32] employs only the first term (ηj); this yields reconnection via resistive diffusion through an elongated current sheet. In space and laboratory plasmas, in which the collision rate is small, the Sweet-Parker model is unable to explain the fast rates of reconnection observed; however, due to

its simplicity, it remains a useful reference scenario for experimental and theoretical investigations.

In other theoretical work, fast reconnection was accounted for by introducing an anomalously high resistivity, η^*, which speeds the rate of magnetic field diffusion. It was argued that the anomalous resistivity stems from instabilities that are produced by the relative streaming of electrons and ions in current layers. The scattering of the electrons in the associated electric field would enhance the drag on the electrons and facilitate an anomalously high rate of momentum transfer between the ions and electrons [33]. For experimental studies, detailed theoretical predictions are available which describe the level and type of turbulence needed to explain fast reconnection [34, 35].

In recent years, the effect of the Hall-term, $\mathbf{j} \times \mathbf{B}/(ne)$, and the related dispersive waves have been studied intensely [35]. In the absence of a magnetic guide field (a magnetic field along the x- line), these analytical and numerical studies indicate that the Hall-term may play a key role in fast reconnection. The ions are thought to be unmagnetized at length scales of the ion skin depth c/ω_{pi}, while the electrons are magnetized down to the electron skin depth, c/ω_{pe}. At length scales smaller than c/ω_{pi}, the Hall term is important through the presence of characteristic in-plane currents. Due to the dispersion relation of the associated dispersive waves, the reconnection rate becomes insensitive to the mechanism that is responsible for breaking the "frozen-in law" [36]. In the presence of a guide magnetic field, not only the Hall term, but also effects related to the electron pressure tensor $\mathbf{p}_e$, are expected to be important [37, 38]. In most reconnection models, the ion sound Larmor radius, $\rho_s = (m_i T_e)^{1/2}/qB$, becomes the characteristic length scale for pressure perturbations in the X-line region. The associated asymmetry in the density profile has been related to the physics of the kinetic Alfvén waves [39] and energization of electrons has been documented numerically in the density depleted parts of the separatrix [40, 41].

In general, the pressure tensor is anisotropic and includes off-diagonal elements, which account for a finite plasma viscosity. However, nearly all analytical work on magnetic reconnection relies on the simplifying assumption that the pressure is isotropic so that the pressure terms can be described by a scalar function. This is also the case for most numerical fluid simulations, although examples exist which include anisotropic pressures components ($p_∥$, $p_⊥$), parallel and perpendicular to the magnetic field.

The electron inertia term, $(me/(ne^2))(d\mathbf{j}/dt)$, is important in time dependent models; the convective component, $v \cdot \nabla$, can also be important in steady state [42, 43]. This is the case when the characteristic length scale for the current profile is comparable to the electron skin depth, c/ω_{pe}. In many models this term is crucial in obtaining electron momentum balance at the x-line.

Fluid formulations rely on the ansatz that the particles cannot sample macroscopic length scales in their motion. This is best achieved when the particles are well magnetized, so that their motion perpendicular to the magnetic field is constrained, and when their parallel mean free path is short. This assumption is fundamental in deriving the fluid models from the kinetic equations and may not be fulfilled during collisionless reconnection. On the other hand, with the development of computational tools and resources, the number of investigations that use particle simulations has increased dramatically. Particle codes simulate the plasma from first principles and are, therefore, likely to capture the important physics for reconnection. Potentially, the boundary conditions applied will impact the results of the simulations, so an important detail of such simulations is to specify realistic boundary conditions. Periodic boundary conditions are the most popular choice owing to their numerical stability and simplicity, but in recent years, codes have been developed that employ so-called "open" boundaries [44].

The appropriateness of the various boundaries remains a subject of controversy. It is likely that the controversy may only be settled through direct observation of reconnection in space or laboratory plasmas. These facts call for caution when applying the fluid models and particle codes to the reconnection problem and call for a careful comparison of theoretical and code predictions with detailed experimental observations in the collisionless domain.

3. Reconnection experiments (from original proposal)

Given that the terms on the R.H. side of equation (1) are associated with length scales that depend differently on the plasma parameters, in principle carefully designed experiments can reveal the conditions under which the various terms become important to the reconnection physics. For this task a number of experiments have been specifically designed in the past [45-53]. Two parameters important for characterizing the experiments are the ratio of the ion Larmor radius to the plasma size (ρ_i/L) and the magnetic Lundquist number $S=\mu_0 L v_A/\eta$, where v_A is the Alfvén speed. A large value of S is required so that the magnetic fields do not to diffuse through the plasma on time scales shorter than the Alven time. The ratio (ρ_i/L) determines whether the ions are magnetized. Some of the early laboratory experiments were based on linear plasma geometries, with $S > 1$, but with (ρ_i/L) > 1 (i.e. un-magnetized ions) [45,47]. In these configurations, the effective plasma resistivity, $\eta^*=E/j$, was observed to be one to two orders of magnitude larger than its classical value. Under these conditions, the anomalous resistivity was found to be caused mainly by turbulence and instabilities. In addition to un-magnetized ions, linear devices are characterized by end effects that introduce additional complications in the interpretation of reconnection results: the electrostatic sheaths at the two ends make determination of the electric field in the body of the plasma difficult due to substantial potential drops in the sheaths.

In the more recent Reconnection Scaling Experiment (RSX) at LANL the 3D merging of two parallel cylindrical flux ropes has been studied. The reconnection process including a strong guide magnetic field was found consistent with Sweet-Parker reconnection [48]. Other recent experiments induce reconnection by merging two spheromak plasma tori. These experiments are characterized by "MHD-like" plasmas, $\rho_i/L<<1$, large Lundquist numbers ($S>100$), and relatively high collisionality ($\lambda_e/L<1$, where λ_e is the electron mean free path). The formation and the evolution of the current layer in the magnetic X-point region is accompanied by the reconstruction of the magnetic flux lines, in space and time, using arrays of internal magnetic probes. The 3D character of magnetic reconnection, including the role of a guide magnetic field in co- and counter-helicity plasma merging, was investigated in the TS-3 experiment [54]. Ion heating and acceleration was observed via Doppler shifts and broadening of plasma spectral lines in [51]. A correlation between magnetic reconnection and the generation of energetic ion flows was found [55]. In the first SSX experiment, two spheromak plasmas interact through cutouts in a wall [53]. This interaction is intrinsically three dimensional, and it reveals an out of plane magnetic field generated by the plasma during the reconnection process [56]. In more recent SSX experiments the characteristic out of plane Hall magnetic fields have been observed, documenting two-fluid effects around the X-line region [57].

In the MRX experiment [52] the plasma is formed by an inductive discharge, and the electric field driving the reconnection is generated by varying the poloidal flux over a short time scale (<50 μs). The experimental investigations indicated that a generalized version of the Sweet-Parker model, including an enhanced resistivity, compressibility, and downstream plasma pressure, could explain the observed geometry of the current sheets. The effective resistivity, measured to be up to a factor of 10 larger than the Spitzer resistivity, enhances as the collisionless regime is approached, i.e. when the mean free path exceeds the thickness of the current sheet. The origin of this enhancement is still not clear. Also in MRX have recent measurements documented the presence of Hall magnetic fields [58].

4. The VTF reconnection experiments

The reconnection experiments at the Versatile Toroidal Facility (VTF) occupy an important niche by exploring reconnection in the collisionless regime for a configuration where the guide magnetic field can be varied continuously. The details of our experimental and theoretical findings are documented in nine Physical Review Letters and several other journal papers [1-24]. The experiments are based on a magnetic geometry including four co-axial coils. The picture in Figure 2(Left) shows these coils during their installation. As illustrated on the RHS diagram, the coils implement a new reconnection drive scenario, where reconnection is driven by transferring the coil current from the center loops to the outer loops.
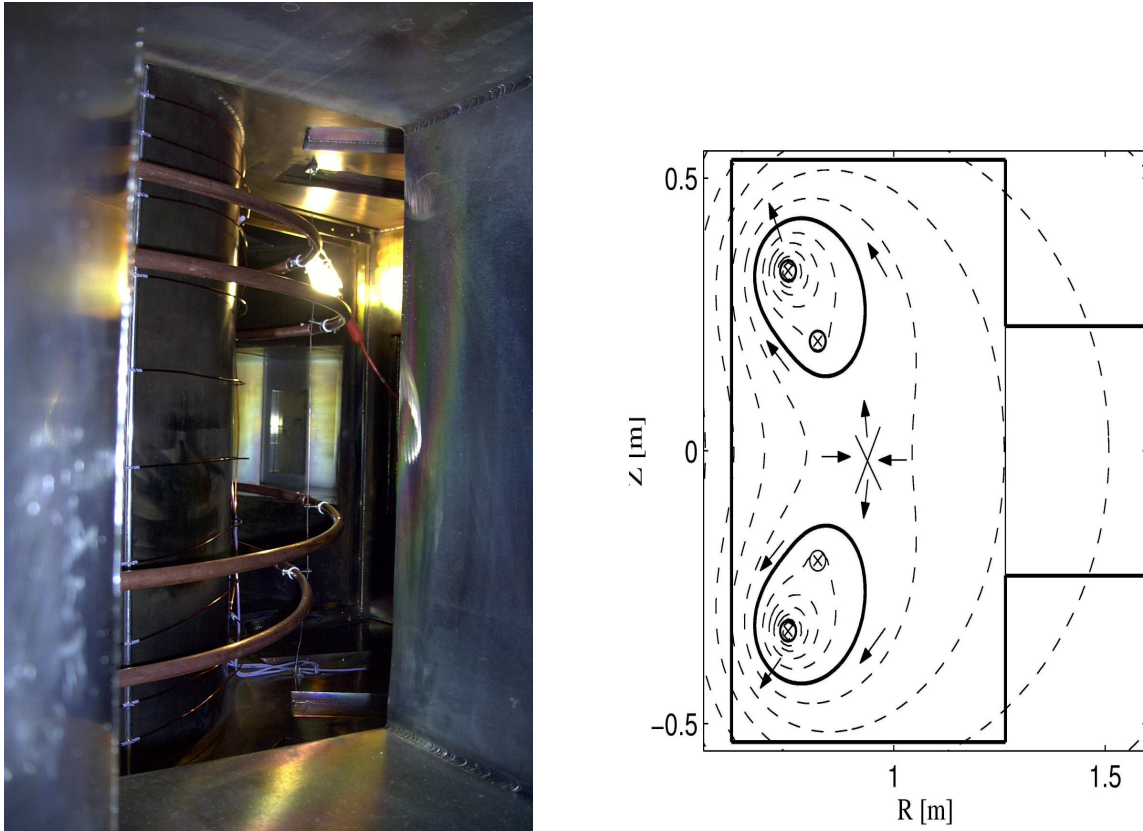

Figure 2. Left: Installation of internal coils implementing a new magnetic geometry. Right: Illustration of the new reconnection drive scenario applied in VTF.

This geometry includes spontaneous reconnection events where the reconnection rate at first is slow and then suddenly transitions into a burst of fast reconnection. As an example Fig.3 documents the evolution of key plasma parameters during spontaneous reconnection. The detail of this event was published in [12] so here we only provide a short description of the data.
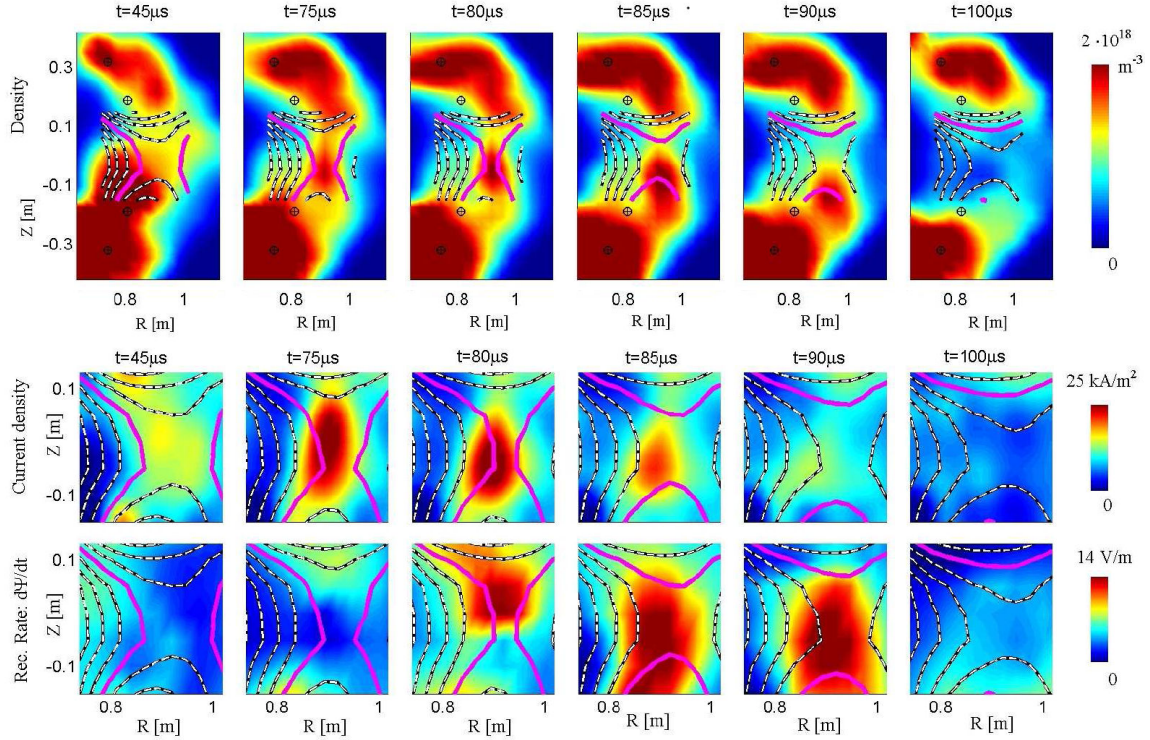
Figure 3. In color, measured contours of the plasma density, floating potential, current density and the reconnection rate. The overlaid lines represent the poloidal projection of magnetic field lines. One set of field lines is highlighted such that the motion of the field lines can be followed in time. The measurements were obtained in a 65μs time interval centered about a spontaneous reconnection event.

The first row if Fig. 3 illustrates the ejection of the plasma density during the reconnection event. As seen in the second and third rows of Fig.3 the reconnection rate spontaneously jumps from 2V/m to 14V/m and coincides with an abrupt decline in the plasma current. This is the first documentation of spontaneous reconnection in a magnetic configuration which initially is toroidally symmetric. The observation of spontaneous reconnection is significant because reconnection as observed in nature is explosive, implying that reconnection must be able to transition from slow to fast; the system must be able to accumulate magnetic stress slowly (in the form of a current sheet), then release it quickly. This is the pattern here reproduced in the VTF experiment.

In experimental configurations where the plasma dynamics is reproducible, magnetic data can be collected in multiple discharges and combined to provide spatially resolved profiles of the plasma dynamics. However, to investigate spontaneous reconnection in VTF, where the reconnection process is not reproducible, all information on the plasma must be collected in a single discharge. For this magnetic flux arrays measure directly the toroidal component of the magnetic vector potential. From this quantity, the magnetic field geometry, current density, and reconnection rate is readily obtained. The details of our new approach to measure the magnetic properties during reconnection were published in Review of Scientific Instruments [13].

The magnetic arrays allow us to measure simultaneously the reconnection rate in two separate toroidal locations. Furthermore, additional arrays measure the magnetic properties of the plasma on the mid-plane of the experiment at 6 different toroidal locations. These measurements show clear evidence of 3D effects in the onset of reconnection. The burst of reconnection starts at one toroidal location, and then propagates around the experiment at the Alfven speed (calculated with the strength of the dominant guide field).
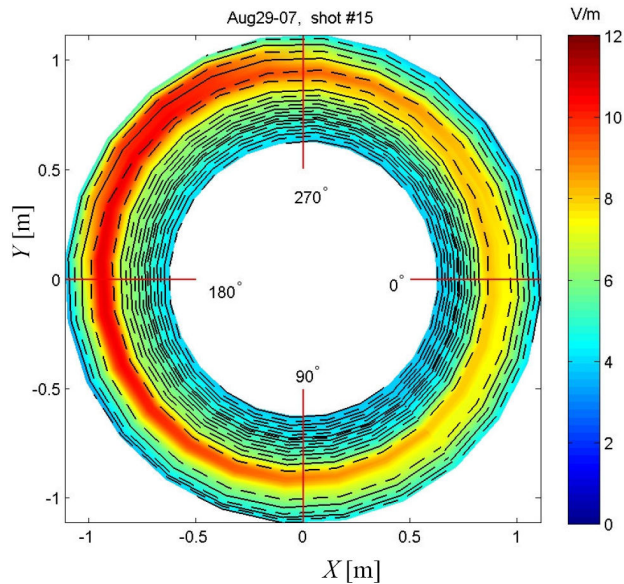
Figure 4. The color contours represent a snapshot in time of the reconnection rate on the midplane of the VTF device. The lines are the intersection of the midplane with magnetic surfaces.

Figure 4 illustrates the effect of the break-down in toroidal symmetry; the reconnection first starts at a toroidal angle of 230 degrees. Throughout the reconnection pulse the flux surfaces at this angle remain further along in the reconnection process resulting in toroidally asymmetric flux surfaces. The implications of these 3D effects are vast. In most numerical simulations of reconnection translational symmetric systems are normally considered, because the full 3D scenario is still intractable even on the most powerful computers (these systems are also known as 2.5D). As a result the magnetic X-line is infinitely long and the main thrust of reconnection research is to understand how this singularity is mitigated by plasma. In contrast to these 2.5D simulations, in our spontaneous reconnection events there exists no true magnetic X-line and there is therefore no singularity.

A more detailed understanding of the 3D dynamics in the onset of reconnection is provided by electrostatic probe measurement. The Fig.5 represents data obtained at a single time by several electrostatic and magnetic arrays. On the right side of Fig. 5 the reconnection electric field is visualized in the midplane of the experiment. This data is measured by six magnetic flux arrays evenly spaced toroidally. The sub-figure clearly shows how reconnection starts at one toroidal angle. By tracking the evolution in time we find that the reconnection dynamics propagate around the experiment at a velocity close to the Alfven speed. The left hand side of the figure shows the density profile, the floating potential, V_f, and the time derivative of the floating potential, dV_f/dt, as recorded at the onset of reconnection. The profiles for $\phi = 270°$ and $\phi = 340°$ illustrate the field evolution on either side of the toroidal location where reconnection begins. An important observation is the asymmetry in dV_f/dt. We find that this asymmetry is fundamental for current continuity: during the reconnection event the toroidal current at one toroidal location decreases abruptly and the requirement for current continuity, $\nabla \cdot \mathbf{J} = 0$, can only be fulfilled by the perpendicular currents having a finite divergence. For this the asymmetric profiles of dV_f/dt drive the required ion currents across the field lines.
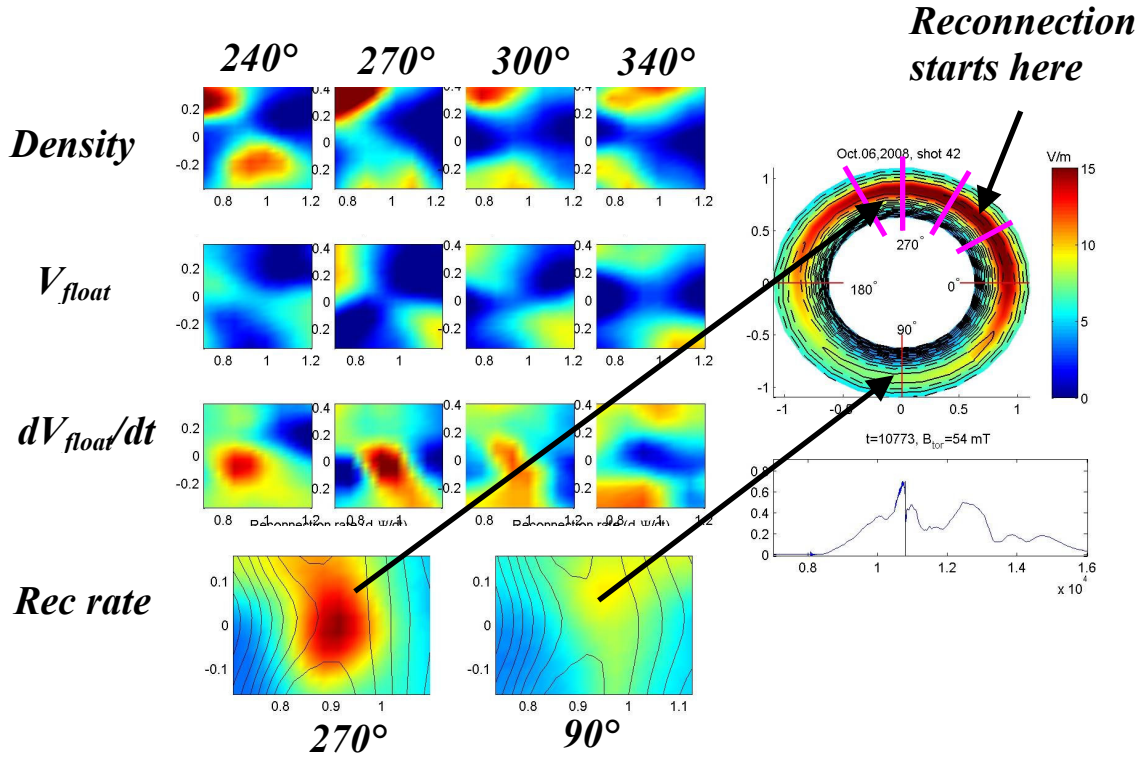
Figure 5. Left: Measured contours of constant plasma density, floating potential, time derivative of the floating potential and the reconnection rate. Right: Top view of the reconnection electric field at the mid-plane of the experiment.

Further evidence of the asymmetry is seen in the electrostatic potential measurements, shown in Fig. 6 also at one time-slice. A global 3D mode arises in conjunction with fast reconnection, and its amplitude increases in time with the reconnection rate. In a previous experiment with toroidal symmetry [19], a quadrupolar axisymmetric potential was found to arise naturally to maintain $\mathbf{E} \cdot \mathbf{B} = 0$ when $\sim$ 5cm away from the x-line. That potential was very similar to that in Fig. 3 measured at the reconnection onset location ($\phi = 270°$). Thus, here too the potential develops to reduce $\mathbf{E} \cdot \mathbf{B}$ in the region of strong toroidal electric field. However, when toroidally away from the onset location, the potential structure rotates with the magnetic field lines, breaking axisymmetry.

The field line rotation can be described using the tokamak safety factor q, the number of times a field line goes around toroidally for one poloidal circuit. We find that fast reconnection is only observed for rational q, specifically when $q \simeq 2$ or $q \simeq 3$ outside the x-line region (see Fig. 6 right). When q is rational, the magnetic field lines close on themselves after only a few toroidal circuits. Rational q is required for the potential mode to develop. The rotating potential is associated with interchange type motion: where q is rational and roughly uniform, flux tubes of plasma can move without bending the magnetic field.
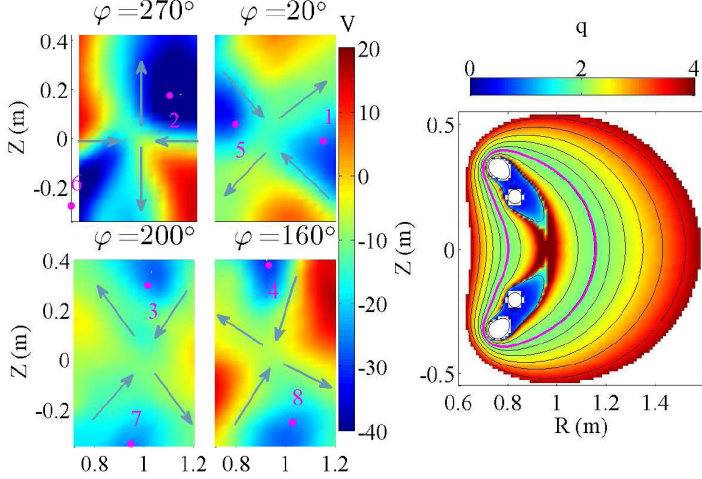
Figure 6: Left: floating potential measured at 4 cross-sections indicated in top row of Fig. 2. Grey arrows represent E×B velocity. Right: $q \simeq 2$ over a large part of the cross-section. The $q \simeq 2$ rotation of the field-aligned potential is evident from the highlighted magenta field line whose sequential puncture-points are shown at left. The rationality of q is required for the potential to map onto itself.

The potential structure of Fig. 6 is essential for explaining current continuity. Asymmetric reconnection implies that the field-aligned current at the x-line no longer closes in toroidal loops. From

$$A_\varphi = \frac{\mu_0}{4\pi} \int \frac{J_\parallel}{|\mathbf{r}' - \mathbf{r}|} d^3 \mathbf{r}',$$

(2)

it follows that a local increase in $-dA_\phi/dt$ must be associated with a local decrease in parallel current density. And since $\nabla_\parallel J_\parallel + \nabla_\perp \cdot J_\perp = 0$, there must be perpendicular currents that compensate for the asymmetry. In our case, these are ion polarization currents, controlled by the potential of Fig. 6. Since for these currents, $J_\perp = (mn/B^2)d\nabla_\perp A_\phi/dt$, we can write the asymmetric part of the parallel current

$$J_\parallel(\mathbf{r}) = J_{\text{edge}} + \int_{\text{edge}}^{\mathbf{r}} \frac{mn}{B^2} \nabla_\perp^2 \frac{\partial \phi}{\partial t} dl$$

(3)

where the integral is evaluated along field lines.

We can use Eq. 3 with a few other observations to model the main features of the 3D reconnection onset. We focus only on the first 10−20μs, i.e. before the inductive electric field propagates around the torus. A cartoon of the model is shown in Fig. 7a. We use the fact that $J_\parallel$ and the electrostatic potential are related by current continuity, the connection between A_ϕ and $J_\parallel$, and an empirical observation regarding Ohm's law to relate A_ϕ to the potential. A combination of all these relations gives an exponentially growing reconnection rate.

To demonstrate this, we substitute Eq. 3 into Eq. 2 and get

$$A_\varphi \simeq \frac{\mu_0}{4\pi} \int \left(\int \frac{mn}{B^2} \nabla_\perp^2 \dot{\phi} dl \right) \frac{d^3 \mathbf{r}'}{|\mathbf{r}' - \mathbf{r}|}.$$

(4)

Next we use the empirical observation that the inductive electric field and the potential mode amplitude grow in time together and we rewrite Eq. 4 as

$$\tilde{A}\bar{\phi} \simeq \left[\frac{\mu_0}{4\pi} \int \left(\int^{\mathbf{r}} \frac{mn}{B^2} \nabla_\perp^2 \tilde{\Phi} dl \right) \frac{d^3 \mathbf{r}}{|\mathbf{r}' - \mathbf{r}|} \right] \ddot{\bar{\phi}}$$

(5)

This equation has the form $f(\mathbf{r})\bar{\phi}(t) = g(\mathbf{r})\ddot{\bar{\phi}}(t)$ which–if $f(\mathbf{r}) \propto g(\mathbf{r})$ and $f/g > 0$–gives exponential growth for ϕ. Figure 7c represents this equation graphically and shows that indeed $f(\mathbf{r})$ and $g(\mathbf{r})$ have similar forms. Then we set $\phi = \exp(\gamma t)$ to find a growth rate of $(27\mu s)^{-1}$, which agrees well with the experimental value of $(25\pm10\mu \, s)^{-1}$, estimated from the time it takes the potential structure of Fig. 6 to develop.

A very similar analysis was carried out in Ref. [6] for toroidally symmetric reconnection. In that experiment, Eq. 2 gave an enhancement in $J_\parallel$ at the x-line, which caused an oscillatory solution $\phi \sim \sin \omega t$. In 3D, the situation is fundamentally different: due to the 3D effects, the increasing ϕ causes a local decrease in $J_\parallel$. This reversal in sign enables the exponentially growing solution $\phi = \exp(\gamma t)$ that we observe [21].
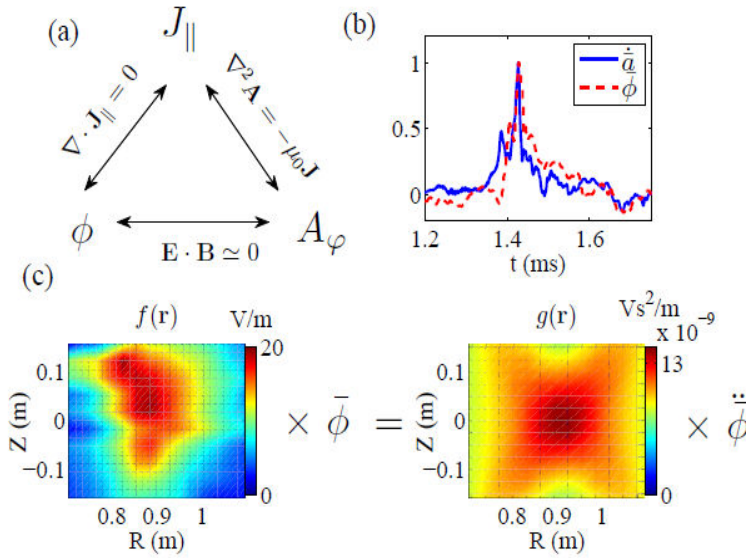

Figure 7: (a) Schematic representation of the model for the reconnection's onset; (b) Mode amplitude (max-min) and peak reconnection rate vs. time; (c) The equation $f(\mathbf{r})\bar{\phi}(t) = g(\mathbf{r})\ddot{\bar{\phi}}(t)$ shown graphically.

5. Electron holes and turbulence during spontaneous reconnection.

Our observations of electron phase-space holes were published in Ref. [16] as a part of the thesis work by W. Fox. Electron phase-space holes [59,60], also called Bernstein-Greene-Kruskal (BGK) solitary structures, are the self consistent plasma structures that form when a finite number of particles become trapped in large-amplitude plasma waves. They play a role in a number of plasma processes, most importantly the nonlinear saturation of velocity-space (two-stream) instabilities. The ''BGK state''—where initial linear modes have evolved into an ensemble of these BGK structures—also appears in the saturation of Landau damping [61]. Electron holes have received substantial attention lately due to a recent generation of spacecraft which has found them to be nearly ubiquitous in the space environment [62,63].

Holes are inherently nonlinear plasma structures, consisting of a positive-potential spike which has trapped a population of electrons. The kinetic, Vlasov description of hole equilibria was established by Bernstein, Greene, and Kruskal [64]. Later, Berk and collaborators showed that these structures appeared in simulations of the two-stream instability when the instability saturated by particle trapping [65]. Recent progress, driven by space observations, has extended

the original 1D theory to higher dimensions, in both dynamical simulations (e.g., [66]) and with analytic equilibria (e.g., [67]), and has established agreement between theory and observations [68]. The dynamics of holes have also been studied in dedicated laboratory experiments [69].

Because of their presence in the turbulent, saturated state of instabilities, electron holes may also play an important role in magnetic reconnection processes. Primarily, current-driven turbulence is studied for its ability to provide ''anomalous resistivity'' to the plasma, speeding the reconnection rate [70]. Drake et al. [71] have found electron holes resulting from electron-ion (Buneman) instability in reconnection simulations and found that they were indeed a source of anomalous resistivity. In space observations, holes associated with reconnection have now been observed both at the bow shock and in the magnetotail [72,73].

Here we discuss the observation of electron holes within the electrostatic turbulence created during spontaneous reconnection events on the VTF. The holes are observed on high-bandwidth, single-ended Langmuir probes as positive spikes of large amplitude. The electron holes are observed in conjunction with the large inductive electric fields and energetic particle creation associated with this magnetic energy release. In contrast to previous laboratory studies [11], where the perpendicular size of the holes was set by the plasma boundary, here the holes are small compared to the size of the experiment, so plasma processes will control the holes' three-dimensional shape. We find that the holes formed are, in fact, 3D structures and are approximately spherical with a scale size of a few electron gyroradii. Our observations also indicate that the holes in VTF most likely arise from electron-electron velocity-space instability.

Figure 8(a) shows a 200 ns trace on a pair of fast Langmuir probes, separated by 4.6 mm in the toroidal direction, essentially parallel to the magnetic field. Fig. 8(b) zooms in on a smaller 10 ns window which contains two spike pairs. The data points, sampled at 5 GS/s, appear as open symbols. The spikes are well correlated between the two probe tips, with a time delay of about 1.2 ns. Other tests with the probes separated perpendicular to the magnetic field show zero time delay, indicating that the spikes travel along the magnetic field. Finally, in Fig. 8(b), the green trace with square symbols is from the ''upstream'' probe—upstream in terms of the electron flow inferred from the total plasma current— indicating that the spikes travel along the magnetic field with the electron flow.
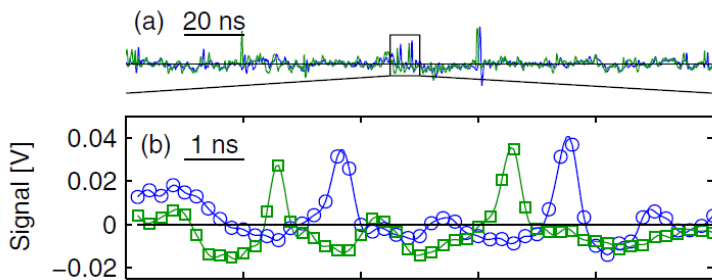

Figure 8: (a) A pair of fluctuation traces over a 200 ns window and (b) a 10 ns window. The probes are separated by 4.6 mm parallel to the magnetic field.

6. Equation of state for guide-field reconnection

Another set of significant results is derived from a new theoretical model for the electron dynamics during reconnection [17], which was inspired by experimental observation in VTF. In the following paragraphs we described how this theory was born out of the experimental observations. Our experimental work on VTF has shown that trapped electrons often play a fundamental role in the observed reconnection dynamics [6]. Based on this insight gained from the experiment we analyzed the electron data of a reconnection event observed by the Wind spacecraft in the deep magnetotail. Our analysis proved that the inner reconnection region is positively charged causing all thermal electrons to follow trapped trajectories. These trajectories have profound implications, as they catalyze fast magnetic reconnection [9]. We use Liouville's theorem together with the single particle constants of motion to derive a simple analytical form for the electron distribution function inside the reconnection region [15].
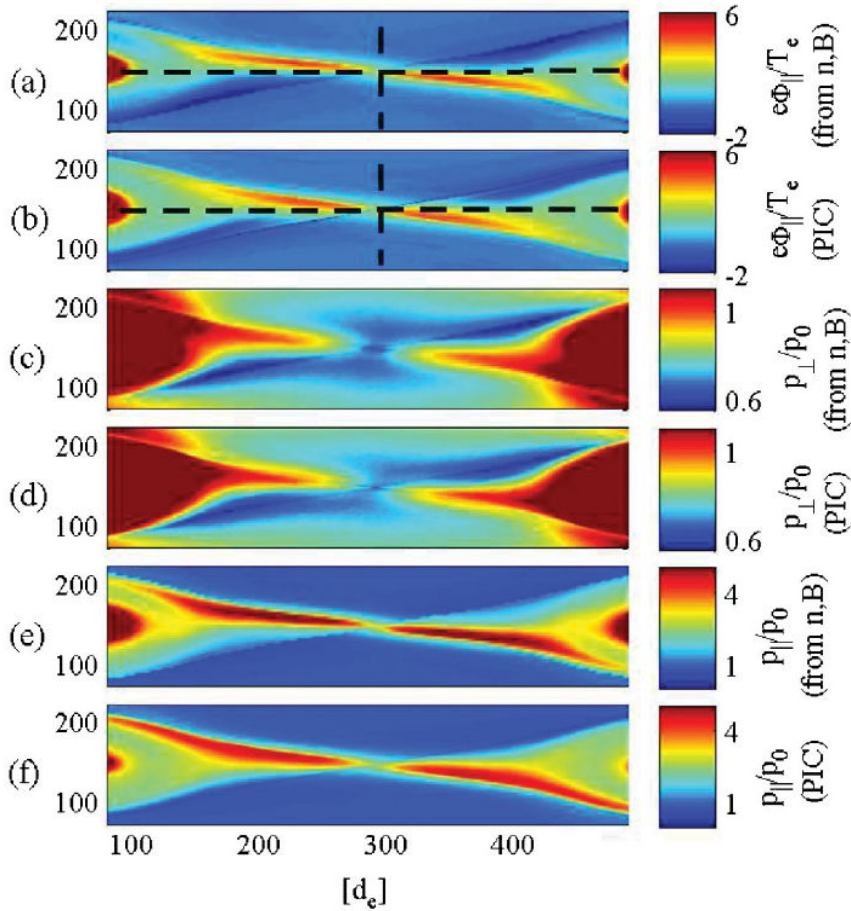

Figure 9: Comparison of fluid model and PIC simulation. Acceleration potential predicted by model and (b) given by integral definition with the integration constant chosen so both match along the dashed lines. (c) Fluid model $p_\perp$, (d) simulation $p_\perp$, (e) fluid model $p_\parallel$, and (f) simulation $p_\parallel$.

In collaboration with Dr. W Daughton at Los Alamos National Laboratory and Prof. J Drake at the University of we have validated our theory directly against their numerical

distribution functions [17,19]. Furthermore, by taking moments of the electron distributions, we have derived new equations of state for the parallel and perpendicular electron pressures. The model allows a fluid description in the collisionless regime where parallel electric fields and the dynamics of both passing and trapped electrons are essential [20] (see Fig. 9). We believe that these new equations of state will have significant impact on the field of reconnection, because they allow fluid simulations to accurately model the electron pressure tensor. This is important because the gradient in the parallel pressure is proportional to the reconnection rate. So far most fluid theories apply an isothermal scaling p=nT, which we find underestimates the parallel pressure often by more than a factor of ten. Thus, besides providing an analytical understanding of the electron dynamics, we foresee that our new model will allow for more realistic numerical modeling of complex systems such as the Earth's magnetosphere. The good agreement between the adiabatic theory and the measured electron distribution functions shows that trapping of electrons in parallel electric field dominates the properties of the electron fluid within the inflow region.

7. Scaling laws for anti-parallel reconnection

As mentioned above, for the case where the electrons are magnetized a complete fluid theory can be obtained by taking moments over the analytical form for the electron distribution function. Le et al. [19] showed that in the inflow region where electron trapping is extensive the parallel and perpendicular electron pressures obey CGL-like equations of state: $p_\parallel \propto n^3/B^2$ and $p_\perp \propto nB$.
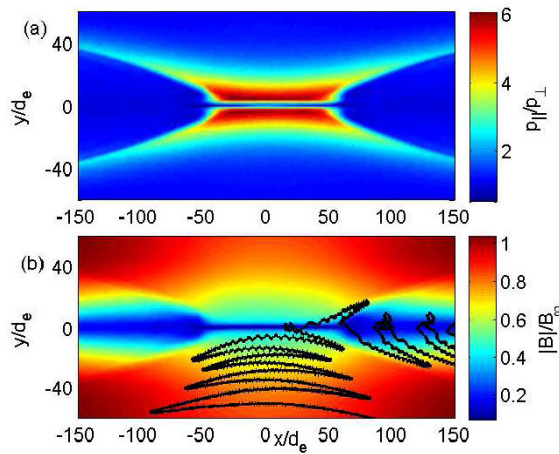

Figure 10: (a) Electron anisotropic pressure ratio $p_\parallel/p_\perp$ from a kinetic simulation of reconnection. (b) Typical trapped electron orbit, which passes repeatedly through the region of weak magnetic field (blue areas) in the outflow.

The strong pressure anisotropy predicted by these equations of state affects electron momentum balance in the inner electron diffusion region. Here, the electrons carry essentially all of the current and correspondingly all of the $j \times B$ force exerted by the magnetic field on the plasma. We highlight the role of the pressure anisotropy by writing steady-state electron momentum balance in the form

$$0 = \nabla_i \left[(B^2/2 + p_\perp)\delta_{ij} + (p_\parallel - p_\perp - B^2)b_i b_j \right] + F_i \ ,$$

where F_i contains the electric field, non-gyrotropic pressure, and inertia contributions. Due to the substantial current in the electron diffusion regions, the magnetic field lines are strongly curved

and $\nabla_i b_i b_j$ is large. The magnetic tension force across the layer associated with the bent field lines, is largely balanced by the anisotropic electron pressure, such that just outside the electron diffusion region $p_\parallel - p_\perp - B^2 \approx 0$.

By combining this condition with the equations of state Le et al. [19,20] derived a scaling law for the strength of the Hall magnetic fields

$$\frac{B_H}{B_\infty} \simeq \left(\frac{\pi n^3 \beta_{e\infty}}{12 n_\infty^3} \right)^{1/4} .$$

This scaling law shows that the electron pressure anisotropy is fundamental in regulating the Hall current system and controls the internal structure of the electron diffusion region. By inserting the value of B_H back into the equations of state scaling laws for $p_\parallel / p_\perp$ and the acceleration potential are obtained. As shown if Fig. 11 these scaling laws has been verified directly against numerical simulations.
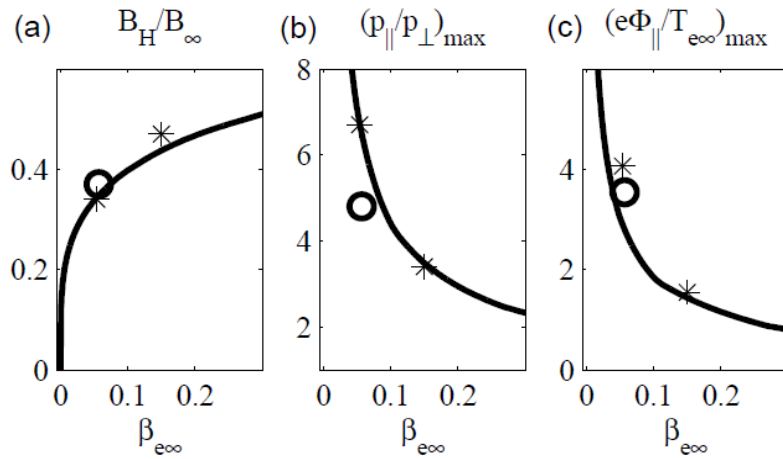

Figure 11: Predicted dependence on upstream electron beta e∞ of various quantities along with PIC simulation results (O, P3d; *, open-boundary code). (a) Characteristic Hall magnetic field strength BH normalized to upstream reconnecting field. (b) Maximum pressure ratio $p_\parallel / p_\perp$. (c) Maximum upstream acceleration potential normalized to electron temperature.

8. Propagation of plasma filaments

Finally we have investigated the propagation of intermittent plasma structures (or blobs) which are relevant to a range of plasmas including the ionosphere and the edge of magnetic fusion devices. The applied experimental geometry is toroidally symmetric, and the filaments, or 'blobs', expand to larger radius, their motion driven by charge build-up at their top and bottom. The charge build-up, which is caused by ∇B and curvature drifts in a 1/R magnetic field, is counteracted by collisional damping on the neutral gas through charge transfer collisions. The blob's electrostatic potential structure and the resulting E × B flow-field give rise to a vortex pair and a characteristic nonlinear mushroom shape, which we observe experimentally for the first time. We also found that blob velocity is inversely proportional to the neutral density, and decreases with time as the blob cools.

The mushroom shape is displayed in Fig. 12, which shows the propagation of a typical blob in poloidal cross section. The time step between adjacent density plots is 100 μs and the first plot occurs 25 μs after the microwaves are turned off. The blob shape exhibits 'wings', which develop about a blob length away from the creation region. A simulation result due to O.E. Garcia shows the same nonlinear blob shape at the lower-right of Fig. 4 for comparison. The upper-right part of Fig. 4 shows the floating potential with some overlayed density contours. The potential is obtained by combining data from a vertical array and a horizontal array. Our findings were published in Physical Review Letters [14].
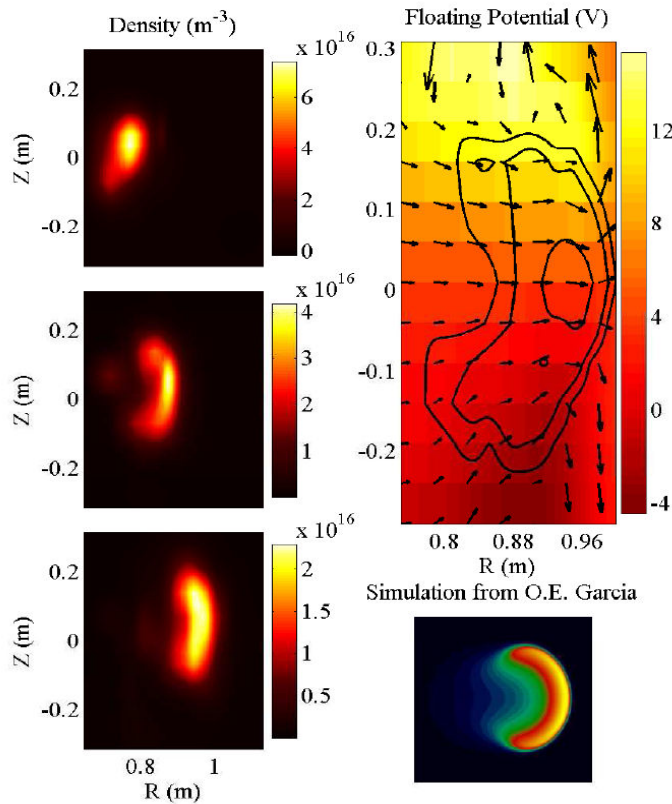

Figure 12: Poloidal cross section of typical blob at 3 different times (Δt = 100μs), showing characteristic mushroom shape. The density is calculated from ion saturation current; its decrease is consistent with the expansion of the blob. The blob propagation is driven by charge build-up, which is reflected in the potential structure at right. The overlaid E × B velocity arrows show the velocity field of a vortex pair. At lower-right is the density from simulation results by O.E. Garcia.

9. Outlook: Three dimensional effects in the onset of fast reconnection

The continued operation of the facility has been secured by an NSF junior faculty award for Prof. Egedal. In addition Profs. Egedal is also seeking to renew an NSF/DOE award to continue the studies initiated over the past funding period. At present, the main focus of the experiment is the three dimensional plasma dynamics observed in the onset of fast reconnection.

References (papers published under this grant are in bold)

[1] J. Egedal, A. Fasoli, M. Porkolab and D. Tarkowski, "Plasma generation and confinement in a toroidal magnetic cusp", Rev. Sci. Instrum. 71, 3351, (2000).

[2] J. Egedal, A. Fasoli, D. Tarkowski and A. Scarabosio, "Collisionless magnetic reconnection in a toroidal cusp", Physics of Plasma, 8, 1935, (2001).

[3] J. Egedal and A. Fasoli, "Single-particle dynamics in collisionless magnetic reconnection", Phys. Rev. Lett., 86, 5047, (2001).

[4] J. Egedal and A. Fasoli, "The topology of guiding center orbits in a linear magnetic cusp", Physics of Plasmas, 8. 4042, (2001).

[5] J. Egedal, "A drift kinetic approach to reconnection in an open cusp plasma", Physics of Plasmas, 9, 1095, (2002).

[6] J. Egedal, A. Fasoli and J. Nazemi, "Dynamical Plasma Response during Driven Magnetic Reconnection", Phys. Rev. Lett. 90, 135003, (2003).

[7] J. Egedal, W. Fox, M. Porkolab and A. Fasoli, "Experimental evidence of fast reconnection via trapped electron motion", Physics of Plasmas, 11, 2844, (2004).

[8] J. Egedal, W. Fox, E. Bolonohy and M. Porkolab, "Kinetic simulation of the VTF magnetic reconnection experiment", Computer Physics Communications, 164, 29, (2004).

[9] J. Egedal, M. Oieroset, W. Fox and RP. Lin, "In situ discovery of an electrostatic potential, trapping electrons and mediating fast reconnection in the Earth's magnetotail", Phys. Rev. Lett. 94, 025006, (2005).

[10] J. Egedal, W. Fox, M. Porkolab and A. Fasoli, "Eigenmode response to driven magnetic reconnection in a collisionless plasma", Physics of Plasmas, 12, 052107, (2005).

[11] A. Stark, W. Fox, J. Egedal, et al., "Laser-induced fluorescence measurement of the ion-energy-distribution function in a collisionless reconnection experiment ", Phys. Rev. Lett. 95, 235005, (2005).

[12] J. Egedal, W. Fox, N. Katz, M. Porkolab, K. Reim, E. Zhang, "Laboratory Observation of Spontaneous Magnetic Reconnection", Phys. Rev. Lett. 98, 015003, (2007).

[13] A. Kesich, J. Bonde, J. Egedal, W. Fox, R. Goodwin, N. Katz, and A. Le, "Magnetic flux array for spontaneous magnetic reconnection experiments", (2008) *Rev. Sci. Instrum*. 79, 063505.

[14] N. Katz, J. Egedal, W. Fox, A. Le, M. Porkolab, "Experiments on the Propagation of Plasma Filaments", (2008) *Phys. Rev. Lett.* 101, 015003.

[15] J. Egedal, W. Fox, N. Katz, M. Porkolab, M. Øieroset, R.P. Lin, W. Daughton, and J.F. Drake, "Evidence and theory for trapped electrons in guide field magnetotail reconnection", (2008) *J. Geophys. Res.,* 113, A12207.

[16] W. Fox, M. Porkolab, J Egedal, N. Katz, A. Le, "Laboratory Observation of Electron Phase-Space Holes during Magnetic Reconnection", (2008) *Phys. Rev. Lett*. 101, 255003.

[17] A. Le, J. Egedal, W. Daughton, W. Fox, N. Katz, "The Equations of State for Collisionless Guide-Field Reconnection", (2009) *Phys. Rev. Lett*. 102, 085001.

[18] J. Egedal, W. Daughton, J.F. Drake, N. Katz, A. Le, "Formation of a localized acceleration potential during magnetic reconnection with a guide field.", (2009) *Physics of Plasmas* 16, 050701.

[19] A. Le A, J. Egedal, W. Daughton, J.F. Drake, W. Fox, N. Katz, "Magnitude of the Hall Fields during magnetic reconnection", (2010) accepted by GRL.

[20] A. Le A, J. Egedal, W. Fox, N. Katz, A. Vrublevskis, W. Daughton, and J.F. Drake, "Equations of state in collisionless magnetic reconnection", (2010) accepted for publication in PoP.

[21] **N. Katz N, J. Egedal, W. Fox, A. Le, J. Bonde, and A. Vrublevskis, "Laboratory Observation of Localized Onset of Magnetic Reconnection", (2010) submitted to PRL.**

[22] **W. Fox, M. Porkolab, J. Egedal, N. Katz, and A. Le, "Laboratory observations of electron energization and associated lower-hybrid and Trivelpiece-Gould wave turbulence during magnetic reconnection", (2010) submitted to PoP.**

[23] J. Egedal, A. Le, N. Katz, L.-J. Chen, B. Lefebvre, and W. Daughton, "Cluster Observations of Bi-directional Beams Caused by Electron Trapping During Anti-parallel Reconnection", (2009) accepted for publication in J. Geophys. Res.

[24] J. Egedal J, A. Le, Y. Zhu, W. Daughton, M. Oieroset, T. Phan, R.P. Lin, J. Eastwood, "Cause of Super-thermal Electron Heating during Magnetotail Reconnection", (2009) submitted to GRL**.**

[25] J. W. Dungey, Phil. Mag. **44**, 725 (1953).

[26] J. B. Taylor, Rev. Mod. Phys. **28**, 243 (1986).

[27] V. M. Vasyliunas, Rev. Geophys. Space Phys. **13**, 303 (1975).

[28] T. D. Phan, et. al Nature **404**, no.6780, pp.848-50 (2000).

[29] S. Masuda, T. Kosugi, H. Hara and Y. Ogawara, Nature **371**, 495 (1994).

[30] R. M. Kulsrud, Phys. Plasmas **2**, 1735 (1995).

[31] P. A. Sweet, Nuovo Cimento Suppl. **8**, Ser. X, 188 (1958).

[32] E. N. Parker, J. Geophys. Res. **62**, 509 (1957).

[33] B. Coppi and A. B. Friedland, Astrophys. J. **29**, 379 (1971).

[34] J. Heyvaerts, E. Priest, and D. Rust, Astrophys. J. **216**, 123 (1977).

[35] J. Birn, J. F. Drake, M. A. Shay, et al., J. Geophys. Res. **106** (A3), 3715 (2001).

[36] M. A. Shay, J. F. Drake, B. N. Rogers and R. E. Denton, Geophys. Res. Lett. **26**, 2163 (1999).

[37] A. Aydemir, Phys. Fluids B **4**, 3469 (1992).

[38] R. Kleva, J. Drake, and F. Waelbroeck. Phys. Plasmas **2**, 23 (1995).

[39] B. N. Rogers, R. E. Denton, J. F. Drake, and M. A. Shay, Phys. Rev. Lett. **87**, 195004 (2001).

[40] J. F. Drake, M.A. Shay, W. Thongthai, et al., Phys. Rev. Lett. **94**, 095001 (2005).

[41] P. L. Pritchett, Phys. Plasmas **12**, 062301 (2005).

[42] J. A. Wesson, Nuclear Fusion **30**, 2545 (1990).

[43] F. Porcelli, D, Borgogno, F. Califano, et al., **44**, 389 (2002).

[44] P. L. Pritchett, J. Geophys. Res. **106** (A11), 25961 (2001).

[45] D. Overskei and P. A. Politzer, Phys. Fluids **19**, 683 (1976).

[46] G. G. Zukakishvili, I. F. Kavartskhava and L. M. Zukakishvili, Sov. J. Plasma Phys. 4, 405 (1978).

[47] R. L. Stenzel and W. Gekelman, J. Geophys. Res. **86**, 649 (1981).

[48] I. Furno, T.P. Intrator, E.W. Hemsing EW, S.C. Hsu, S. Abbate, P. Ricci,and G. Lapenta, Phys. Plasmas **5**, 055702 (2005).

[49] A. T. Altyntsev, V. M. Bardakow, V. I. Krasov, N. V. Lebedev and V. L, Paperni, Solar Phys. 106, 131 (1986).

[50] S. V. Bulanov and A. G. Frank, Sov. J. Plasma Phys. **18**, 797 (1992).

[51] Y. Ono, M. Yamada, T. Akao, T. Tajima and R. Matsumoto, Phys. Rev. Lett. **76**, 3328 (1996).

[52] M. Yamada, H. T. Ji, S. Hsu, T. Carter, R. Kulsrud, N. Bretz, F. Jobes, Y. Ono and F. Perkins, Phys. Plasmas **4**, 1937 (1997).

[53] M. R. Brown, Phys. Plasmas **6**, 1717 (1999).

[54] Y. Ono, M. Inomoto, T. Okazaki and T. Ueda, Phys. Plasmas **4**, 1953 (1997).

[55] T. W. Kornack, P. K. Sollins and M. R. Brown, Phys. Rev. E **58**, R36 (1998).

[56] M. R. Brown, C. D. Cothran, M. Landreman, et al., Phys. Plasmas **9**, 2077 (2002).

[57] C.D. Cothran, M. Landreman, M.R. Brown, J. Matthaeus, J. Geophys. Res. **32**, 3105 (2005).
[58] Y. Ren, M. Yamada, S. Gerhardt, et al., Phys. Rev. Lett. **95**, 055003 (2005)
[59] I. Bernstein, J. Greene, and M. Kruskal, Phys. Rev. 108, 546 (1957).
[60] H. Schamel, Phys. Rep. 140, 161 (1986).
[61] J. R. Danielson et al., Phys. Rev. Lett. 92, 245003 (2004).
[62] H. Matsumoto et al., Geophys. Res. Lett. 21, 2915 (1994).
[63] R. E. Ergun et al., Phys. Rev. Lett. 81, 826 (1998).
[64] D. S. Montgomery et al., Phys. Plasmas 9, 2311 (2002).
[65] K.V. Roberts and H. L. Berk, Phys. Rev. Lett. 19, 297 (1967).
[66] M. Oppenheim et al., Phys. Rev. Lett. 83, 2344 (1999).
[67] C. S. Ng et al., Phys. Plasmas 13, 055903 (2006).
[68] M. Goldman et al., Phys. Rev. Lett. 99, 145002 (2007).
[69] K. Saeki et al., Phys. Rev. Lett. 42, 501 (1979).
[70] H. Ji et al., Phys. Rev. Lett. 92, 115001 (2004).
[71] J. Drake et al., Science 299, 873 (2003).
[72] H. Matsumoto et al., Geophys. Res. Lett. 30, 1326 (2003).